The turbulent bottom Ekman boundary layer measured over a continental shelf

Y. Yoshikawa,[1] T. Endoh,[1] T. Matsuno,[1] T. Wagawa,[2] E. Tsutsumi,[3]

H. Yoshimura,[4] and Y. Morii[4]

[1]Research Institute for Applied Mechanics, Kyushu University, Kasuga, Fukuoka, Japan.

[2]Tohoku National Fisheries Research Institute, Fisheries Research Agency, Miyagi, Japan.

[3]Graduate School for Science and Technology, Kyushu University, Kasuga, Fukuoka, Japan.

[4]Faculty of Fisheries, Nagasaki University, Nagasaki, Japan.

An acoustic Doppler current profiler was deployed in summer and autumn in 2007–2009 at two stations on the East China Sea shelf. Clear velocity spirals that basically correspond to theoretical Ekman spirals were identified for both mean and tidal currents. From these spirals and the corresponding Ekman equation, we estimated the time-averaged eddy viscosity (μ) profiles. The estimated μ was largest (2–3 $\times$ 10^{-3} m^2 s^{-1}) around 5 m from the bottom and decreased almost exponentially with height. A qualitatively similar profile of the eddy diffusivity was also inferred from the acoustic Doppler current profiler data and microstructure profiler data. The flux Richardson number was estimated as 0.11$\pm$0.10 $\sim$ 0.46$\pm$0.17, indicating relatively large buoyancy contribution to the turbulent kinetic energy budget.

1. Introduction

Strong tidal currents over a large continental shelf such as the East China Sea (ECS) induce an intense vertical shear near the shelf floor. Shear-generated turbulence enhances vertical mixing, transporting water properties near the sea floor (such as high nutrient concentrations) upward. The mixing thickens the bottom Ekman boundary layer in which across-shore Ekman transport is induced by along-shore geostrophic currents. In the ECS, the northeastward Kuroshio along the shelf break induces onshore transport that could transport nutrients from deeper layers of the Kuroshio region onto the shelf. Thus, tidal currents and turbulence have large impact on biochemical processes in the shelf region.

Large tidal currents form a logarithmic boundary layer near the shelf floor (e.g., *Lueck and Lu* [1997]; *Lozovatsky et al.* [2008]). In that layer, the eddy viscosity (μ) increases linearly with height from the bottom. As the height increases further, the effect of the Earth's rotation (the Coriolis acceleration) becomes large and the Ekman layer, in which shear-generated turbulence tends to be suppressed, is formed. Density stratification also suppresses the shear-generated turbulence. Consequently, μ should decrease with height in the Ekman layer. Although several observational studies have investigated μ profile in the Ekman layer (e.g., *Werner et al.* [2003]; *Book et al.* [2009]), these studies relied on turbulence closure model. *Sakamoto and Akitomo* [2008] conducted direct numerical simulations for idealized tidal flows, but the Reynolds number is lower than the real one. Thus μ profile in the Ekman layer remains uncertain and should be investigated with an alternative approach.

We deployed an acoustic Doppler current profiler (ADCP) on the shelf floor of the ECS, which revealed velocity spirals that basically correspond to bottom Ekman spirals. This allowed us to assume an Ekman balance near the bottom and solve for a time-averaged μ profile that best fits measured spirals in a least-square sense. Together with measurements of dissipation rates of turbulent kineitc energy and density with a microstructure profiler, we also inferred the eddy diffusivity (κ) profile. In the remainder of this paper, data are described in section 2, measured current structures and estimated profiles of μ and κ are described in section 3, and concluding remarks are given in section 4.

2. Data

An ADCP was deployed at two stations (Fig. 1) in different years. At station 1 (31° 45'N, 127° 25'E, 128 m depth), an ADCP (RDI, Workhorse 300 kHz) was deployed during October 11–16 (5.5 days) in 2007 and during August 19–October 17 (60 days) in 2008. At station 2 (31° 45'N, 125° 30'E, 60 m depth), an ADCP (RDI, Workhorse 600 kHz) was deployed during July 18–24 (6.5 days) in 2009.

At station 1 (2), velocities were measured from 4.6 (2.6) m to at least 80 (30) m height above the bottom with a 2 (1) m bin size. Both ADCPs were set in a trawl-resistant bottom mount (Floating Tech, AL200) to minimize unfavorable damage from trawling. Ping intervals were less than 3 s. The hourly averaged velocity was used in this study. Tidal harmonic analysis of the hourly velocity was performed to obtain tidal harmonic coefficients and the mean current velocity. For 2008 data, a total of 29 tidal components were analyzed. Dominant tidal components were M_2, S_2, O_1 and K_1 with major (minor) axis amplitudes of 0.24 m s^{-1} (0.11 m s^{-1}), 0.12 m s^{-1} (0.06 m s^{-1}), 0.07 m s^{-1} (0.06 m s^{-1})

and 0.05 m s^{-1} (0.05 m s^{-1}), respectively. For 2007 and 2009 data, only M_2 and O_1 tidal currents were analyzed due to the limited observation period.

Dissipation rates of kinetic energy (ϵ) along with water temperature and salinity were estimated using a microstructure profiler (Alec Inc., TurboMAP) near station 1 (Fig. 1) during October 14–16 in 2007. The TurboMAP profiler was cast three or four times every hour for the 2.5 days starting from 07:00 on October 14. Hourly ϵ and water density were estimated by averaging respective values calculated from each single cast. Details of the estimation procedure are the same as those given by *Endoh et al.* [2009].

3. Results

3.1. Vertical Current Structure

Figure 2 shows the velocity structure of the mean current, the semidiurnal (M_2) tidal current, and the diurnal (O_1) tidal current. In this figure, tidal currents are represented by velocity vector at the time when the velocity at 30 m from the bottom is largest. All the tidal currents rotate anticyclonically with time at all depths. Noteworthy is that rapid deflections of the current direction with depth are obvious near the sea floor. (Exceptions are the diurnal tidal current in 2007 and the mean current in 2009 due to contamination by near-inertial internal waves and the small velocity, respectively.) Further noteworthy is that both the mean and diurnal tidal currents deflect cyclonically with depth (with decreasing height), while the semidiurnal tidal currents deflect anticyclonically with depth.

These features are consistent with classical Ekman theory. The velocity spiral caused by each rotary component of the interior current with frequency ω (cyclonic is positive)

under the assumption of constant eddy viscosity μ_0 is (e.g., *Kundu et al.* [1981])

$$u + \imath v = (U_I + \imath V_I) \exp(\imath\omega t) \left(1 - \exp\left(-(1 \pm \imath)\frac{z}{\delta_E}\right)\right) \quad \text{for} f + \omega \gtrless 0 \tag{1}$$

$$\delta_E = \left(\frac{2\mu_0}{|f + \omega|}\right)^{1/2}, \tag{2}$$

where $\imath = (-1)^{1/2}$, f ($= 7.65 \times 10^{-5}$ s^{-1}) is the Coriolis parameter, $(u + \imath v)$ is the velocity caused by the interior current $(U_I + \imath V_I) \exp(\imath\omega t)$, and δ_E is thickness of the boundary layer induced. Note that a current of one tidal constituent is given by a sum of cyclonic ($\omega > 0$) and anticyclonic ($\omega < 0$) rotary components. Thus, the anticyclonic component of the semidiurnal tidal current ($\omega = -1.45 \times 10^{-4}$ s^{-1} $\equiv -\omega_2$) induces anticyclonic deflection with depth, whereas the cyclonic component of the semidiurnal tidal current ($\omega = +\omega_2$), both components of the diurnal tidal currents ($\omega = \pm 7.27 \times 10^{-5}$ s^{-1} $\equiv \pm\omega_1$) and the mean current ($\omega = 0$) induce cyclonic deflection.

In Figure 2, hodographs of the above analytical solution (a sum of the anticyclonic and cyclonic solutions of Eq. 1) are also plotted. These hodographs are obtained by matching the analytical velocity with the measured velocity at 7 m above the bottom with tentative value of μ_0 ($= 10^{-3}$ m^2 s^{-1}). The good agreement between the measured and analytical hodographs indicates that the currents are in approximate Ekman balance.

3.2. Vertical Profile of Eddy Viscosity

Although the measured and theoretical hodographs are similar, the differences are not small if velocities at each depth are compared. This is due mainly to the unrealistic assumption of the constant eddy viscosity.

In this study, we estimated μ profile from the measured velocity profiles. Here, the time-averaged μ was investigated, though it should vary with time in actuality. The profile of

μ can be estimated by solving the Ekman equation written as

$$\imath(f+\omega)w_E = \frac{\partial}{\partial z}\left(\mu(z)\frac{\partial}{\partial z}w_E\right), \tag{3}$$

where $w_E = u_E + \imath v_E$ is each boundary-layer rotary component of the current with frequency ω. The boundary condition we use is

$$\mu\frac{\partial w_E}{\partial z} = 0 \text{ at } z = z_T. \tag{4}$$

The boundary layer component of the velocity (w_E) was defined as the measured velocity (w_M) minus the interior component of the velocity (w_I) (i.e., $w_E = w_M - w_I$). The boundary component is set as zero ($w_M = w_I$) above the top of the boundary layer (z_T). Judging from Fig. 2, we can reasonably set z_T as 25 m. Note that the following results are not so sensitive to the choice of z_T as long as 20 m $\leq z_T \leq$ 30 m. The interior component (w_I) of the mean currents was assumed to be linearly sheared, while the interior component of the tidal currents was assumed to be vertically uniform. The interior shear of the mean currents is determined such that the root-mean-square difference between w_M and w_I is minimized above z_T.

We assume that turbulence in the bottom Ekman layer is local and μ is represented by real numbers. Thus, there are a total of 10 equations (x and y components (real and imaginary parts, respectively) of the equations for $\omega = 0$ (the mean current), $\pm\omega_1$ (the diurnal tidal currents), and $\pm\omega_2$ (the semidiurnal tidal currents)) for a single profile of $\mu(z)$. Thus, the least-squares technique can be used to estimate $\mu(z)$.

Given that km is the number of vertical grid levels and mm ($= 10 \times km \times$ the number of datasets) is the total number of Ekman equations, the finite-difference version of equation 3 and 4 can be written as $\mathbf{A}\mu = \mathbf{b} + \mathbf{e}$, where $\mathbf{A}$ is a $km \times mm$ matrix containing

coefficients on the right-hand side of equation (3), $\mu = (\cdots, \mu_k, \cdots)^T$ is a km column vector representing the eddy viscosity profile, $\mathbf{b}$ is an mm column vector determined from the left-hand side of equation (3), and $\mathbf{e}$ is an error vector representing neglected higher order terms. The eddy viscosity profile that minimizes $\mathbf{e}^T\mathbf{e}$ under the assumption of $\mathbf{A}$ with no error can be obtained as $\mu = (\mathbf{A}^T\mathbf{A})^{-1}\mathbf{A}^T\mathbf{b}$. For finite difference, the second-order central scheme was used. (The fourth-order scheme provides similar results.)

The estimated μ is still subject to an estimation error in tidal harmonics which contaminates $\mathbf{A}$ and $\mathbf{b}$. An ADCP measurement error is one source of this error. Uncertainty level of μ due to the ADCP measurement error was estimated from an ensemble of μ obtained by repeating the above analysis (beginning from tidal harmonic analysis) of 512 sets of hourly ADCP velocity with artificial random noise whose standard deviation was set as 2.0 cm s^{-1} (e.g., *Yoshikawa et al.* [2007]). Short measurement periods (> 5.5 days) are other possible source of the tidal harmonic errors. However, the largest frequency resolution ($1/5.5$ days$^{-1} = 2.1 \times 10^{-6}$ s^{-1}) is smaller than $f + \omega$ for most cases and hence effects of this error is less significant. (Exception is the anticyclonic diurnal tidal current ($f + \omega = 3.8 \times 10^{-6}$ s^{-1}), but its contribution to the estimated μ was found small.)

Eddy viscosities at stations 1 and 2 were separately estimated. Data obtained in 2008 (measurement period of 60 days) were divided into eight sub-datasets (each record length being 7 days) and tidal harmonic analysis for M_2 and O_1 only was performed for each dataset. A total of nine datasets (one of 2007 data and eight of 2008 data) were used to estimate one eddy viscosity profile at station 1. At station 2, a single dataset was used to estimate μ.

Figure 3 shows the estimated μ and its uncertainty level (standard deviation of the ensemble) at stations 1 and 2. At both stations, the estimated μ was largest ($\simeq$ 2–3 $\times 10^{-3}$ m^2 s^{-1}) at 3–7 m height from the bottom, and decreased almost exponentially with height above. At station 2, μ was almost constant below 5 m. This implies a boundary between the logarithmic layer (in which μ increases linearly with height) and the Ekman layer (in which μ decreases with height) at about 5 m height with some areas of overlap a few meters thick. The exponential decay was slightly faster at station 1 than station 2, perhaps due to a difference in density stratification between two stations.

We also estimated μ profiles for spring and neap tides separately. In this estimation, datasets for station 1 were separately analyzed for spring tide (five datasets) and neap tide (four datasets). The shapes of the estimated profiles (dashed and dashed-dotted lines in Fig. 3) were similar, and the averaged μ at spring tide is 2.1 times larger than at neap tide. This is in fair agreement with the scaling analysis of the eddy viscosity $\mu \propto U_*^2/|f+\omega| \propto (U_I^2+V_I^2)/|f+\omega|$ (e.g., *Sakamoto and Akitomo* [2008]) because the major-axis amplitudes at spring tide were 1.7 ($= (2.9)^{1/2}$) times those at neap tide.

3.3. Vertical Profile of Eddy Diffusivity

Figure 4 shows the shear production ($SPR = \mu(z)((\partial u/\partial z)^2 + (\partial v/\partial z)^2)$) of turbulent kinetic energy (TKE) calculated from the measured velocity (u, v) (not tidal harmonic coefficients) and the estimated μ during October 11–17 in 2007, along with the dissipation rates (ϵ) of the TKE and density (ρ) measured with TurboMAP during October 14–16 in 2007. In general, SPR was larger than ϵ. Temporal variations of SPR were more smooth than those of ϵ owing to the use of the time-averaged μ. Note also that the difference

between SPR and ϵ was larger where density stratification was larger. Thus, the difference seems to be ascribed largely to the buoyancy production (BPR) of the TKE. BPR can be expressed as $BPR = -\kappa(g/\rho)\partial\rho/\partial z$, where κ is the eddy diffusivity and g (=9.8 m s^{-2}) is the gravitational acceleration. Assuming $\partial\mathrm{TKE}/\partial t = SPR + BPR - \epsilon = 0$ at each height (e.g., *Burgett et al.* [2001]), we can infer κ from SPR, ϵ, and ρ. Uncertainty level of SPR was calculated from a propagated ADCP measurement error, while that of ϵ was examined by creating 512 profiles of ϵ with artificial random noise whose standard deviation is set as the standard deviation of ϵ calculated from single cast in a corresponding hour. The inferred profile of κ and its uncertainty level are shown in Fig. 3. The profile is basically similar to that of μ, and κ is one-order smaller than μ above 10 m height. Though κ is less certain than μ, similarity in κ and μ profiles and reasonable range of κ indicate the overall validity of the present estimation.

Note that the time-averaged flux Richardson number ($R_f = (SPR - \epsilon)/SPR$) was estimated as 0.11±0.10 (23 m height) $\sim$ 0.46±0.17 (at 11 m height). Thus our estimate of R_f near the bottom was larger than the typical value of 0.17 (e.g., *Thorpe* [2007]) which is often used for estimating κ from a microstructure profiler. This indicates that quantitative evaluations of R_f are necessary for more quantitative estimation of κ in the bottom Ekman boundary layer over a continental shelf.

4. Concluding Remarks

Velocity spirals of the mean flow detected at station 1 are direct evidence of the onshore Ekman transport in the ECS. From vertical integration of w_E (along with linear interpolation from the lowest measurement level to the nonslip bottom), the onshore transports

per unit area are estimated as 0.33 m^2 s^{-1} (2007) and 0.13 m^2 s^{-1} (2008). Assuming the flow at station 1 extends along an isobath of 1000 km length in the ECS, these correspond to 0.13 $\sim$ 0.33 Sv (1 Sv$\equiv$ 10^6 m^3 s^{-1}). This is comparable to the volume fluxes of the Kuroshio Tropical and Intermediate Waters (0.24–0.26 Sv) onto the ECS (*Chen and Wang* [1999]), indicating significant roles of the bottom Ekman transport.

We estimated time-averaged μ and κ. However, they should vary in time according to the temporal variation in the tidal current velocity. Different density stratifications at the two stations might be responsible for different profiles of μ at the stations. To investigate these effects, more detailed field measurements are required. Numerical experiments will also be useful to investigate such effects. These are the aims of our future study.

Acknowledgments. We thank an anonymous reviewer for comments. This study is supported in part by the Special Coordination Funds for Promoting Science and Technology ("Establishment of Cooperative Sea Under Common Understanding of the Marine Environment of the East China Sea") and by a Grant-in-Aid for Scientific Research (B) from the Ministry of Education, Culture, Sports, Science, and Technology (22340140).

References

Book, J. W., P. J. Martin, I. Janekovic, M. Kuzmic, and M. Wimbush (2009), Vertical structure of bottom Ekman tidal flows: Observations, theory, and modeling from the northern Adriatic, *J. Geophys. Res. Oceans*, *114*, C01S06, doi:10.1029/2008JC004736.

Burgett, R. L., D. Hebert, and N. S. Oakey (2001), Vertical structure of turbulence on the southern flank of Georges Bank, *J. Geophys. Res. Oceans*, *106*(C10), 22,545–22,558.

Chen, C. A., and S. L. Wang (1999), Carbon, alkalinity and nutrient budgets on the East China Sea continental shelf, *J. Geophys. Res. Oceans*, *104*(C9), 20,675–20,686.

Endoh, T., T. Matsuno, Y. Yoshikawa, Y. Tatsuyama, and J. Ishizaka (2009), Observations of wind-driven deepening of the surface mixing layer in the Tsushima Strait, *J. Oceanogr.*, *65*, 273–279.

Kundu, P. K., J. O. Blanton, and M. M. Janopaul (1981), Analysis of current observations on the Georgia Shelf, *J. Phys. Oceanogr.*, *11*, 1139–1149.

Lozovatsky, I., Z. Liu, H. Wei, and H. J. S. Fernando (2008), Tides and mixing in the northwestern East China Sea part II: Near-bottom turbulence, *Cont. Shelf Res.*, *28*, 338–350.

Lueck, R. G., and Y. Lu (1997), The logarithmic layer in a tidal channel, *Cont. Shelf Res.*, *17*(14), 1785–1801.

Sakamoto, K., and K. Akitomo (2008), The tidally induced bottom boundary layer in a rotating frame: similarity of turbulence, *J. Fluid Mech.*, *615*, 1 – 25.

Thorpe, S. A. (2007), *An Introduction to Ocean Turbulence*, 240 pp., Cambridge university Press.

Werner, S. R., R. C. Beardsley, and S. J. Lentz (2003), Observations and modeling of the tidal bottom boundary layer on the southern flank of Georges Bank, *J. Geophys. Res. Oceans*, *108*(C11), doi:10.1029/2001JC001271.

Yoshikawa, Y., T. Matsuno, K. Marubayashi, and K. Fukudome (2007), A surface velocity spiral observed with ADCP and HF radar in the Tsushima Strait, *J. Geophys. Res. Oceans*, *112*, C06022, doi:10.1029/2006JC003625.

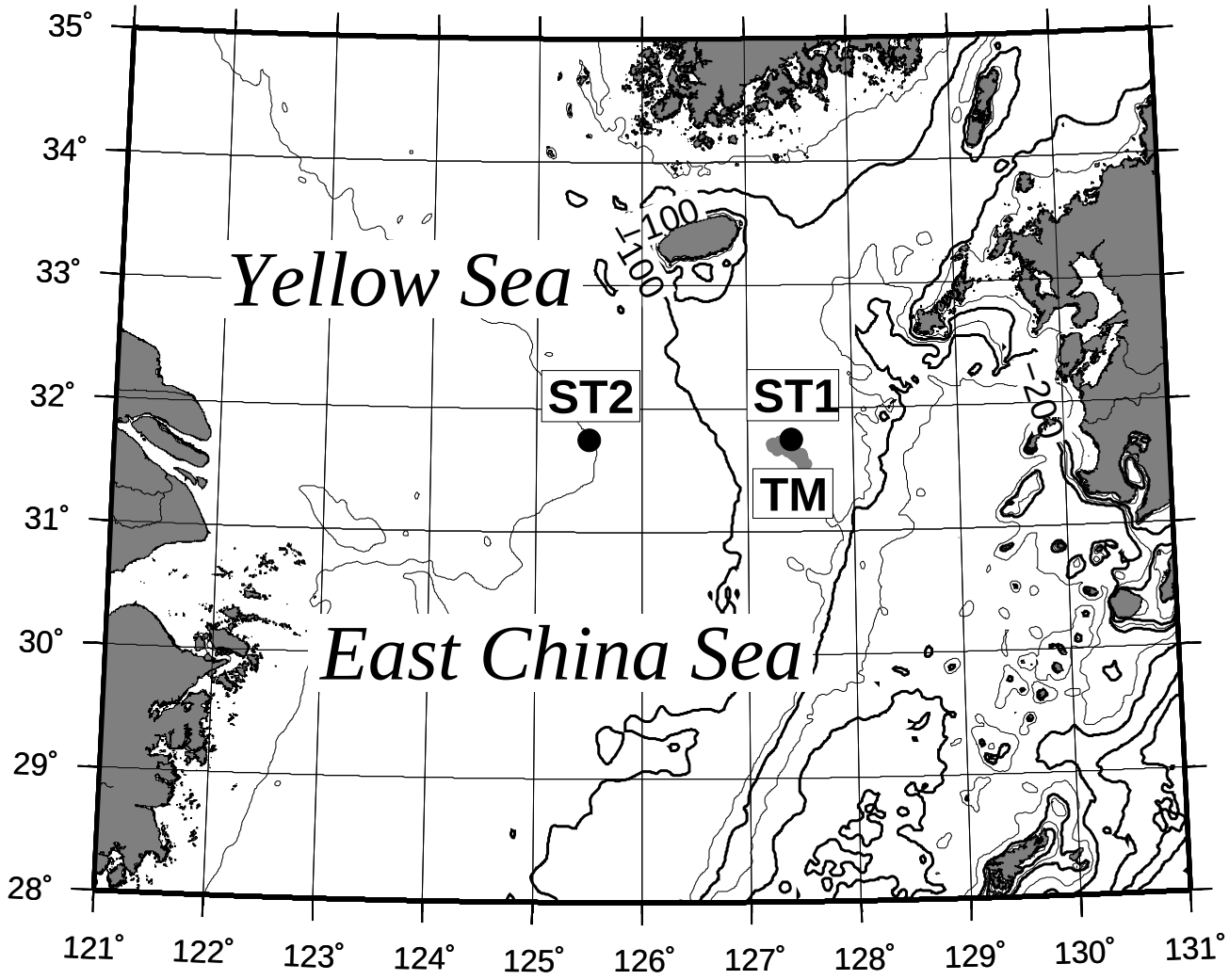

Figure 1. Locations of the ADCP stations (ST1 and ST2). Gray dots to the southwest of ST1 denote the locations of TurboMAP measurements (TM).

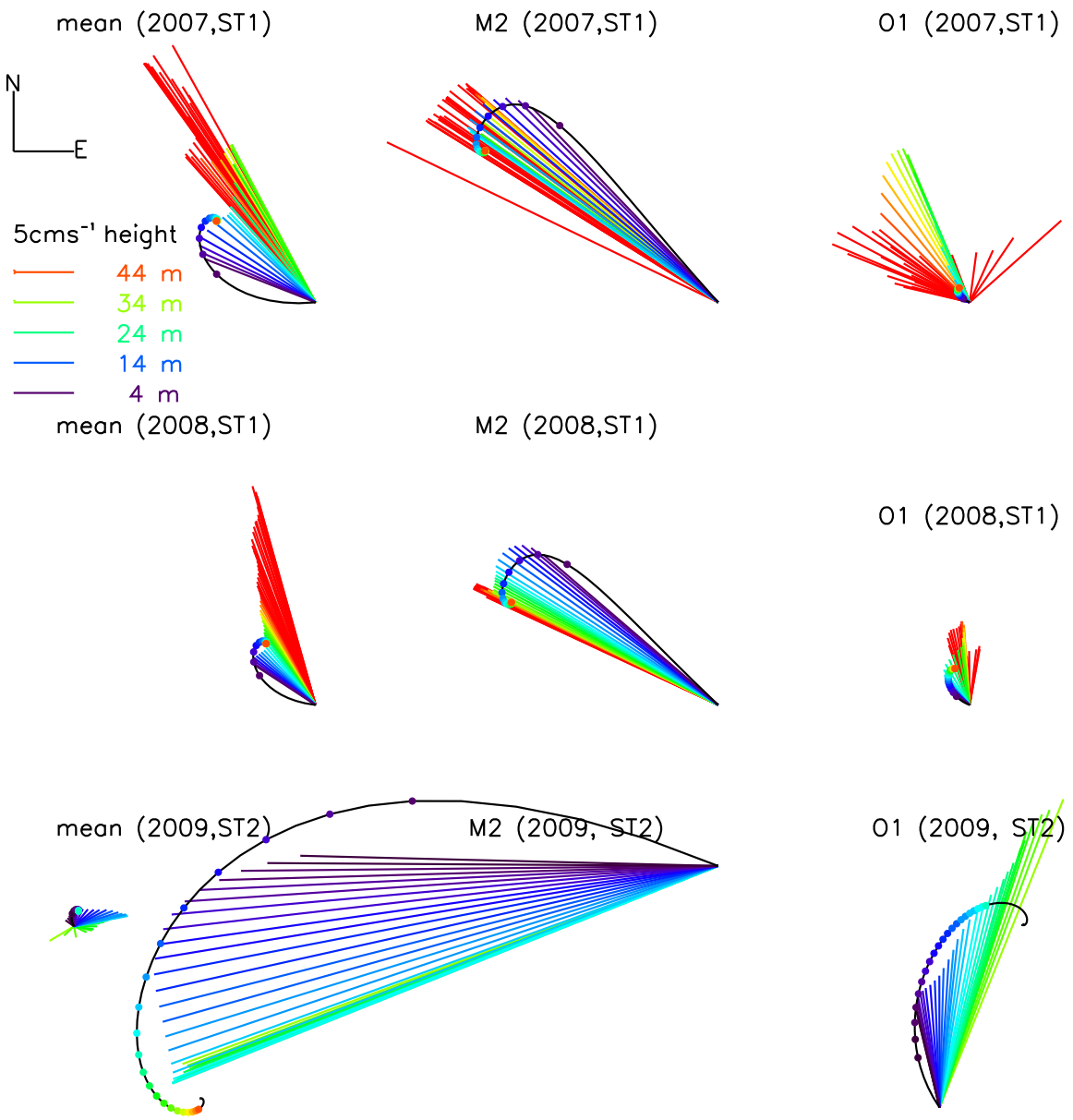

Figure 2. Vertical structure of mean currents (left), semidiurnal tidal currents (center) and diurnal tidal currents (right) estimated from ADCP data obtained in 2007 (upper), 2008 (middle) and 2009 (lower). Note that tidal currents are represented by velocity vector at the time when the velocity at 30 m from the bottom is largest. Color represents height from the bottom. Hodographs of the corresponding Ekman spirals are also shown by sold lines, with colored dots representing the height from the bottom.

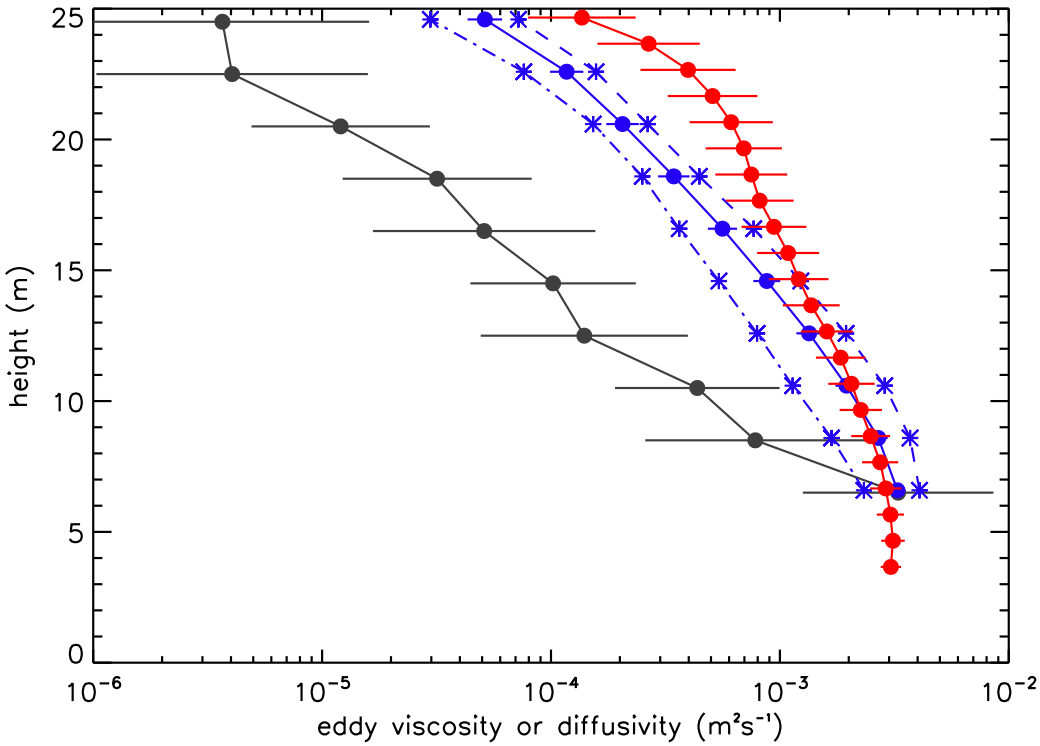

Figure 3. Profiles of μ estimated from velocity spirals observed at station 1 (blue) and station 2 (red). Blue dashed and dashed-dotted lines represent the profiles for spring and neap tides, respectively. The gray solid line represents κ estimated from ADCP and TurboMAP data obtained during October 14–16. Horizontal bars denote the standard deviation calculated from an ensemble of μ or κ.

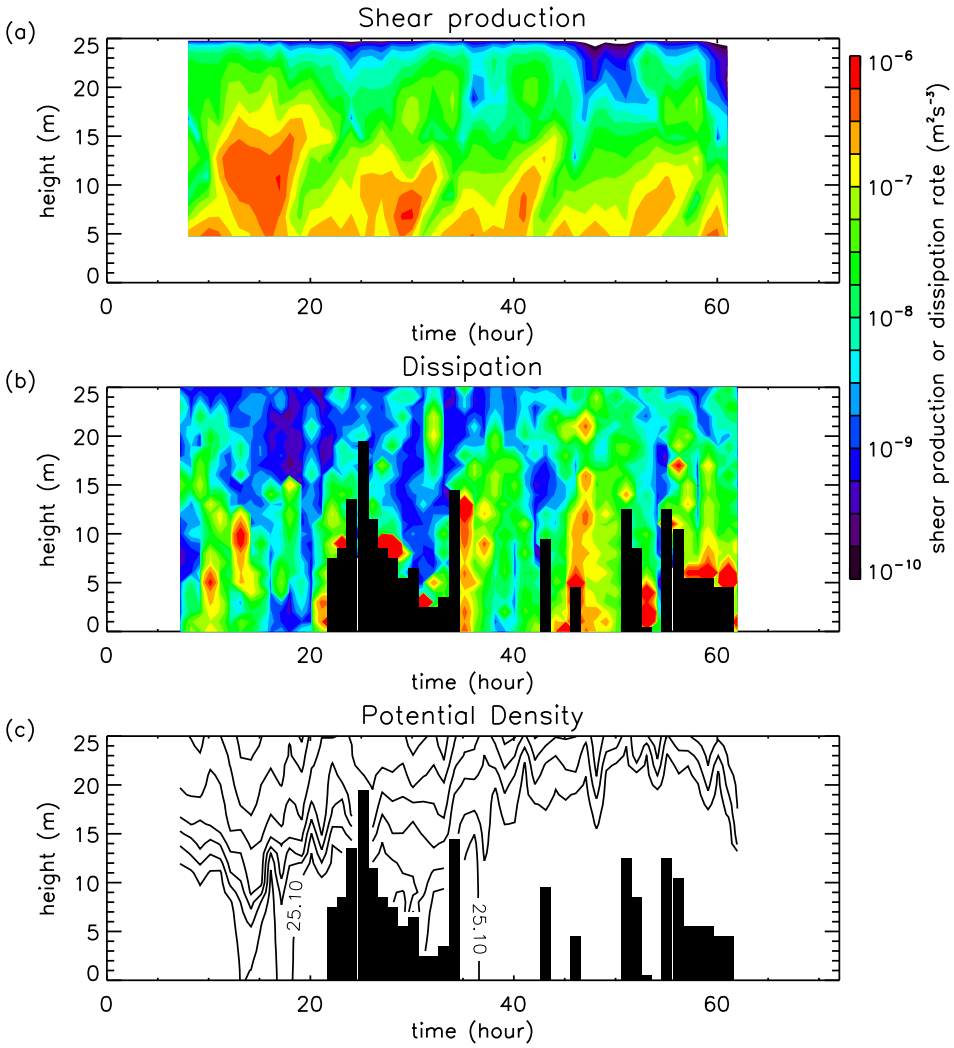

Figure 4. (a) Shear production of the TKE estimated by the ADCP. (b) Dissipation rate of the TKE estimated by the TurboMAP profiler. (c) Water density ($\rho - 1000$ kg m^{-3}) measured by the TurboMAP profiler (contour interval is 0.1 kg m^{-3}). The horizontal axis is the time (hour) from 0:00 on October 14 and the vertical axis is the height from the bottom. Black solid regions in (b) and (c) represent missing data.